Comparison of the semiclassical and modified semiempirical method of spectral calculation

D. J. Heading,[1] J. S. Wark,[1] R. W. Lee,[2] R. Stamm,[3] and B. Talin[3]
[1]*Department of Physics, Clarendon Laboratory, University of Oxford, Parks Road, Oxford, OX1 3PU, United Kingdom*
[2]*Lawrence Livermore National Laboratory, Livermore, California 94551*
[3]*PIIM, Université de Provence, Centre Saint Jérôme, URA 773 Case 232, 13397 Marseille Cédex 20, France*
(Received 12 August 1996; revised manuscript received 7 March 1997)

In recent experiments the capacity has been developed to generate plasmas at high densities. Standard methods used to diagnose plasmas are difficult to apply at these conditions, since it is necessary to calculate the entire spectrum as there is significant overlap of spectral lines. However, for most elements, the number of individual spectral line profiles calculated using the semiclassical method is very small. We present a method to use an approximate line width formula, coupled with an accurate database to generate a large number of line profiles. We evaluate the accuracy and utility of such an approach by comparison with semiclassical calculations. [S1063-651X(97)10307-5]

PACS number(s): 52.70.Kz, 32.70.Jz

I. INTRODUCTION

In recent years the potential for obtaining high energy-density plasma sources, i.e., plasmas having high density and relatively high temperature, that could be created reproducibly in the laboratory has been realized [1–3]. These sources are at sufficiently extreme conditions that the standard methods of plasma spectroscopic diagnosis are untested and must be validated before confidence in their use is achieved. Here we report on the development of a model that is intended to test the level of accuracy that one can ascribe to the observables in such an experiment. In particular we look at the case of a warm dense metal plasma in a regime where the concept of an individual line shape or line intensity breaks down.

In standard plasma spectroscopy the use of individual spectral line shapes as a diagnostic of plasma conditions is a well-known and widely used technique for both astrophysical and terrestrial plasmas. Line shapes are extremely useful as they represent the classic noninterfering probe of the plasma. The shape and intensity of the lines reveal the various aspects of the plasma environment; ion temperature (Doppler thermal effect), electron density (Stark effect), and velocity fields (Doppler motional effect) are commonly inferred plasma parameters from spectral line analysis. Furthermore, temperature measurements can be carried out by measuring the relative intensity of spectral lines from two different ionization stages. Although this does not require a knowledge of the detailed line shapes, the intensity of the line wings must be considered. These techniques become increasingly difficult as the electron density increases, and as the lines broaden and merge in wavelength space. Hence density diagnosis from a single line is not reliable at high densities, and temperature diagnosis becomes increasingly difficult. It is the plasma spectroscopy of this regime that we will evaluate here.

The preponderance of line shapes is normally calculated from the semiclassical models developed by Griem and Baranger [4,5], and yet there are comparatively few spectral lines for which semiclassical calculations have been performed. This is due to the difficulty of obtaining accurate atomic structure data and performing electron–atom-scattering calculations. Since the semiclassical calculations are computationally expensive, they have been performed only for a restricted set of strong lines for a given element. This leaves the situation for astrophysical plasmas, and increasingly for terrestrial plasmas, unsatisfactory in that the available line shapes are not sufficient for diagnosis of higher-density plasmas.

The situation is made worse for these higher densities, as we have broad, overlapping spectral lines. Selectively calculating spectral features is insufficient, and a different approach to plasma diagnosis is required. Instead of studying only one or two isolated lines to obtain the plasma conditions, an entire section of the spectrum should be observed. All the spectral lines in that region, and others on the edges of the area of interest, have to be included. Account must also be taken of the ionization balance of the plasma, and spectral lines from different ionization stages must also be modeled. Thus line broadening for a variety of spectral lines is required, and the observed intensity is the sum of all contributions from different lines. Hence there is a requirement for a rapid computational method for obtaining spectral line profiles for many transitions. We note that historically this has been the province of the opacity code calculations; however, here we are not interested in energy flow alone but in spectral diagnostics.

This requirement for the rapid calculation of spectral line widths has led to the development of a number of approximate methods [6–10]. Of these, the modified semiempirical method (MSEM) has perhaps received the most attention [6–8,11]. The required atomic data for this method are limited, and simple approximations can be used. Various studies have established that the method yields an accuracy of the linewidth around 50% for most spectral lines [6,9,11]. The structures of the ions of interest are needed in order to calculate the ionization balance and line intensities. Recent work by the Opacity Project [10] has yielded a database of large quantities of atomic data for light elements. This data set can be used to generate simulations of wide spectral regions by use of the MSEM. It is the coupling of this atomic data base with a fast method for estimating linewidths which gives this method it utility and applicability.

TABLE I. Values of $g(x)$ for $x<100$, from [8].

x	$g(x)$
>2	0.2
3	0.24
5	0.33
10	0.56
30	0.98
100	1.33

In this work we present calculations of the visible spectrum of a dense, warm, aluminum plasma. The spectra were calculated both by using data obtained from previous detailed calculations of the line shapes using the semiclassical theory [12], and by using the modified semiempirical method. The latter was used in conjunction with the Opacity Project database for the first four ionization stages of aluminum. This provided the matrix elements, transition wavelengths, energy levels, and degeneracies required for the calculation. Comparisons between the two calculations are made, and also between the calculations and observations from a dense, warm aluminum plasma [1]. Hence an estimate is made of the reliability of spectra calculated using the MSEM and a consistent data set, and the presumably more reliable semiclassical calculation.

II. MODIFIED SEMIEMPIRICAL METHOD

Within the impact approximation, the width of an isolated ion line is given by [5]

$$w=N\left(v\left[\sum_{i'}\sigma_{i'i}+\sum_{f'}\sigma_{f'f}\right]\right)_{\rm av}+w_{\rm el}, \tag{1}$$

where w is the full width at half maximum of the line in angular frequency units, and N is the electron density. $\sigma_{j'j}$ is the inelastic cross section for collisional transitions to states j' from j levels of the optical transition. $w_{\rm el}$ is the line width induced by elastic collisions. The average is over the electron velocity (v) distribution.

Within the dipole approximation we may use Bethe's [13] relation for the inelastic cross section

$$\sigma_{j'j}=\frac{8\pi}{3}\,\lambda\overline{R^2_{j'j}}\,\frac{\pi}{\sqrt{3}}\,g, \tag{2}$$

where g is the Gaunt factor, λ is the reduced de Broglie wavelength, and $\overline{R^2_{j'j}}$ is the square of the coordinate operator matrix element summed over all components of the operator, the magnetic substates of the total angular momentum, and averaged over the magnetic substates.

In the MSEM we assume that the contribution of the elastic collisions at high electron temperatures to the linewidth is negligible [6]. At low temperature, the elastic collisions are taken into account using the threshold value of the inelastic cross section. For $\Delta n=0$ transitions, it is found that the threshold value for the Gaunt factor is too small, and it has been modified for these transitions [8]. The electron impact width of a spectral line may then be written in angular frequency units, as

$$w=N_e\,\frac{8\pi}{3}\,\frac{\hbar^2}{m^2}\left(\frac{2m}{\pi kT}\right)^{1/2}\frac{\pi}{\sqrt{3}}\left[(\overline{R^2_{l_i,l_{i+1}}})_{\Delta n=0}\tilde{g}\left(\frac{E}{\Delta E_{l_i,l_{i+1}}}\right)+(\overline{R^2_{l_i,l_{i-1}}})_{\Delta n=0}\tilde{g}\left(\frac{E}{\Delta E_{l_i,l_{i-1}}}\right)+(\overline{R^2_{l_f,l_{f+1}}})_{\Delta n=0}\tilde{g}\left(\frac{E}{\Delta E_{l_f,l_{f+1}}}\right)\right.$$
$$\left.+(\overline{R^2_{l_f,l_{f-1}}})_{\Delta n=0}\tilde{g}\left(\frac{E}{\Delta E_{l_f,l_{f-1}}}\right)+\sum_{i'}(\overline{R^2_{i'i}})_{\Delta n\neq 0}g\left(\frac{E}{\Delta E_{i'i}}\right)+\sum_{f'}(\overline{R^2_{f'f}})_{\Delta n\neq 0}g\left(\frac{E}{\Delta E_{f'f}}\right)\right], \tag{3}$$

where $\overline{R^2_{l_j,l_{j+1}}}$ is the matrix element between state j and j', n_j is the effective principal quantum number, $E=3kT/2$ is the energy of the perturbing electron, and $\Delta E_{jj'}=|E_{j'}-E_j|$ is the energy difference between levels j and j'. $\tilde{g}(x)$ is the modified Gaunt factor, given by

$$\tilde{g}(x)=0.7-\frac{1.1}{Z}+g(x). \tag{4}$$

$g(x)$ is a tabulated function, and its values are shown in Table I for $x\leqslant 100$ and Z is the charge number ($Z=1$ for neutral). For high temperatures, $x>50$, and an approximation to the Gaunt factor can be used [14]:

$$g(x)=\frac{\sqrt{3}}{\pi}\left[\frac{1}{2}+\ln\left(\frac{2ZkT}{n_1\Delta E_{ll'}}\right)\right]. \tag{5}$$

If the nearest perturbing level is far enough from j or i that the condition $E/\Delta E_{jj'}\leqslant 2$ is satisfied, the matrix elements in Eq. (3) are given by

$$\overline{R^2_{jj}}=\sum_{j'}\overline{R^2_{j'j}}\approx\frac{1}{2}\left(\frac{n_j}{Z}\right)^2[5n_j^2+1-3l_j(l_j+1)], \tag{6}$$

where n_j is the effective principal quantum number, which is given by

$$n_j^2=Z^2\,\frac{E_H}{(I-E_i)}, \tag{7}$$

where E_i is the empirical excitation energy, and I is the ionization energy. When $E/\Delta E_{jj'}\leqslant 2$, $g(x)=0.2$, and the linewidth in Å is then

$$\Delta w(\text{Å}) = 0.443\times 10^{-8}\,\frac{\lambda^2(\text{cm})N_e(\text{cm}^{-3})}{T^{1/2}}\,(\overline{R_{ii}^2}+\overline{R_{ff}^2}). \tag{8}$$

This approximation is simple and fast, but is not particularly accurate or appropriate for many lines, and it still requires the input or calculation of the effective principal quantum number, which itself requires atomic data.

If the condition $E/\Delta E_{jj'} \leqslant 2$ is not satisfied, Eq. (1) can be solved using [8,9]

$$\overline{R_{jj'}^2} \approx \left(\frac{3n}{2Z}\right)^2 \frac{\max(l_j, l_{j'})}{2l+1}\,[n^2 - \max^2(l_j, l_{j'})]\phi^2, \tag{9}$$

where ϕ^2 is the Bates-Damgaard factor [15], tabulated by Oertel and Shomo [16]. The matrix element sum is given by

$$\sum_{j'} (\overline{R_{jj'}^2})_{\Delta n\neq 0} = \left(\frac{3n_j}{2Z}\right)^2 \frac{1}{9}\,(n_j^2 + 3l_j^2 + 3l_j + 11) \tag{10}$$

The nearest perturbing level can be estimated from

$$\Delta E_{n,n+1} \approx \frac{2Z^2E_H}{n^3}. \tag{11}$$

In all cases, atomic data, i.e., energy levels, transition wavelengths, angular momenta, and effective quantum numbers are required. The data are employed in the development of the spectrum, but are also used to determine the level populations. That is, the atomic energy levels are needed to obtain the partition functions required for the Saha-Boltzmann equation, given that local thermal equilibrium is valid at the conditions of interest. This indicates that the use of single, consistent set of atomic data may remove some of the uncertainties in the calculations of the spectrum, and enable a more accurate representation of the plasma spectrum while still giving a rapid approximation to the linewidths of a large number of lines.

III. DATA SET AND CODE

To construct a spectrum, three elements are required. First, atomic data are required for both the structure of the ions and scattering. Second, the ionization balance and level populations need to be calculated. Finally, the spectrum has to be constructed. The spectral construction relies on a series of approximations. These elements are treated below.

A. Atomic data

The atomic structure data was taken from the Opacity Project (OP) [10]. The data are organized into two complementary sets, one dealing with energy levels, and the other with transitions. Each energy level is referenced by two numbers which give a unique reference for that state. One of these, slp, gives the spin, angular momentum, and parity of the level; and the other, n, gives the index of the level in the series. Hence a search can be made for an energy level which is also a state of a transition. All transitions $\Delta l = \pm 1$ for which $n \leqslant 10$ and $l \leqslant 5$ have been calculated with Einstein A coefficients and effective quantum numbers.

Before undertaking the calculation, it is important to know the possible errors which may be induced from the input atomic data. A comparison between the literature values of the wavelengths for some Al I, II, and III lines are shown in Tables II–IV. These indicate that on average the error in wavelength is less than 1%, with a maximum of around 4%. Other comparisons show similar high average accuracy, and so we can be confident that the input data is of high average quality, although we must bear in mind that it is not sufficient for spectroscopic accuracy.

B. Ionization balance

The ionization balance can be calculated from the Saha-Boltzmann equation. For the plasmas of interest, which have non-negligible but small coupling, we find that it is necessary to calculate the full partition function in order to obtain the correct ionization balance. In order to calculate the partition function, an estimate of the degree of ionization potential depression must be made. This is necessary to truncate the summation over states in the partition functions, and also to remove transitions from the calculation which have become bound free. The following uses the Debye model, where the sum is truncated at the electron Debye radius. Other approximations, such as the ion-sphere radius or Stewart-Pyatt model [17] can be used, but they change the spectrum very little [12].

We find with the OP data that the number of transitions contained in the database for a given ion stage is a great deal larger than those for which semiclassical line-shape data are available. Thus, the calculation using the MSEM and OP data includes a much greater total oscillator strength. For example, the total oscillator strength included in the OP data for Al I is 2678.77 summed over all transitions. If we assume a plasma electron density of 2×10^{19} cm^{-3} and temperature of 2 eV, then, using the Debye model, we calculate that of this oscillator strength 23.97 is below the depressed ionization potential. In the calculation based on the semiclassical data [12] we only included lines of $\lambda < 1000$ nm, and for these data, the total available oscillator strength is 0.9026, of which 0.878 is below the depressed ionization potential. As a check we note that if we exclude lines of $\lambda > 1000$ nm in the OP database, we obtain an oscillator strength of 0.901 78, which agrees closely with that for the oscillator strength in the semiclassical calculation.

We will describe below a comparison between the MSEM using the OP database and a calculation based on results from various semiclassical calculations. In the semiclassical case, the energy levels are taken from the literature [18]. It is instructive here to compare results for the ionization balance for the case of the literature values for energy levels, and for that using the OP data. We find that the results for the partition functions for the two calculations vary slightly ($\sim 8\%$ for Al I at 2×10^{19} cm^{-3}, and 25 000 K). We find that the mean ionization Z^* is only $\sim 1\%$ different at these conditions. The atomic data used are only slightly different, and do not significantly alter the ionization balance. The codes have different but similar energy levels, and so this

TABLE II. Half widths at half maximum of some Al I lines, calculated at $N_e = 1 \times 10^{17}$ cm^{-3}, $T_e = 40\,000$ K, for both semiclassical and MSEM calculations. λ_{Lit} is the literature value for the transition [22], λ_{OP} the wavelength calculated by the Opacity Project [10], Δw_{SC} refers to the linewidth calculated from the semiclassical results [7,23], and Δw_{MSEM} refers to the widths calculated using the MSEM and OP database (this work). Configurations were taken from [24]. Powers of 10 are enclosed in brackets.

Transition	λ_{Lit} (nm)	λ_{OP} (nm)	$\frac{\lambda_{OP}}{\lambda_{Lit}}$	Δw_{SC} (nm)	Δw_{MSEM} (nm)	$\frac{\Delta w_{MSEM}}{\Delta w_{SC}}$	Oscillator strength
$3s^2 3p - 3s^2 6d$ $^2P^0$-^2D	220.83	222.9	1.01	7.53[−02]	1.005	13.35	0.066
$3s^2 3p - 3s^2 7s$ $^2P^0$-^2S	226.18	228.4	1.01	3.61[−02]	0.113	3.13	0.003
$3s^2 3p - 3s^2 5d$ $^2P^0$-^2D	226.72	229	1.01	0.304	0.390	1.28	0.098
$3s^2 3p - 3s^2 4d$ $^2P^0$-^2D	237.1	239.7	1.01	0.117	0.112	0.96	0.12
$3s^2 3p - 3s^2 6s$ $^2P^0$-^2S	237.63	240	1.01	0.16	3.07[−02]	0.19	0.004
$3s^2 3p - 3s^2 nd$ $^2P^0$-^2D	257.28	261	1.01	5.29[−02]	2.78[−02]	0.53	0.044
$3s^2 3p - 3s^2 5s$ $^2P^0$-^2S	265.72	268.5	1.01	5.08[−02]	6.10[−03]	0.12	0.014
$3s^2 3p - 3s^2 3d$ $^2P^0$-^2D	308.92	311.2	1.01	2.34[−02]	2.06[−02]	0.88	0.175
$3s^2 3p - 3s^2 4s$ $^2P^0$-^2S	395.57	400.1	1.01	2.05[−02]	3.08[−03]	0.15	0.115
$3s^2 4s - 3s^2 6p$ ^2S-$^2P^0$	555.74	559.9	1.01	1.29	1.12	0.87	0.006
$3s^2 4s - 3s^2 5p$ ^2S-$^2P^0$	669.7	675.2	1.01	0.633	0.334	0.53	0.034
$3s^2 3d - 3s^2 6f$ ^2D-$^2F^0$	783.55	796	1.02	5.18	21.94	4.24	0.079
$3s^2 3d - 3s^2 5f$ ^2D-$^2F^0$	877.34	892.7	1.02	2.33	9.71	4.17	0.17
$3s^2 4p - 3s^2 7s$ $^2P^0$-^2S	883.78	885.8	1.00	5.51	1.88	0.34	0.007

result is expected. Any differences in the spectra from the codes are hence due to the input transition data or to the method of calculation of the linewidths.

C. Spectral construction

To construct the spectrum, we require the central wavelengths of the transitions, the upper-state energy levels and degeneracy, and the dipole matrix element, which is obtained from the Einstein A coefficient. From these data the line width can be calculated in accordance with Eq. (3) above.

The calculation of Eq. (3) was implemented using a FORTRAN code. The linewidths are calculated by searching for the Einstein A coefficient of the $\Delta l = \pm 1$ transitions of the correct parity from the upper and lower states of the transi-

TABLE III. Half widths at half maximum of some Al II lines, calculated at $N_e = 1 \times 10^{17}$ cm^{-3}, $T_e = 40\,000$ K, for both semiclassical and MSEM calculations. λ_{Lit} is the literature value for the transition [22], λ_{OP} the wavelength calculated by the Opacity Project [10], Δw_{SC} refers to the linewidth calculated from the semiclassical results [7,23], and Δw_{MSEM} refers to the widths calculated using the MSEM and OP database (this work). Configurations were taken from [24]. Powers of 10 are enclosed in brackets.

Transition	λ_{Lit} (nm)	λ_{OP} (nm)	$\frac{\lambda_{OP}}{\lambda_{Lit}}$	Δw_{SC} (nm)	Δw_{MSEM} (nm)	$\frac{\Delta w_{MSEM}}{\Delta w_{SC}}$	Oscillator strength
$3s3p$-$3s4d$ $^1P^0$-^1D	153.974	154.8	1.01	1.22[−02]	8.76[−03]	0.72	0.52
$3s3p$-$3s5s$ $^1P^0$-^1S	162.56	164.7	1.01	8.15[−03]	1.29[−03]	0.16	0.014
$3s^2$-$3s3p$ ^1S-$^1P^0$	167.081	164	1.02	2.05[−04]	2.77[−04]	1.35	1.84
$3s3p$-$3s3d$ $^3P^0$-^3D	172.32	171.1	0.99	8.97[−04]	1.62[−03]	1.81	0.901
$3s3p$-$3s4s$ $^3P^0$-^3S	186.03	184.2	0.99	1.85[−03]	1.14[−03]	0.62	0.129
$3s3p$-$3p5d$ $^1P^0$-^1D	199.053	200.1	1.01	4.46[−03]	1.61[−03]	0.36	1.45
$3p^2$-$3s5p$ ^1D-$^1P^0$	247.53	244.8	0.99	3.85[−02]	1.50[−02]	0.39	0.0232
$3s3d$-$3s6p$ ^3D-$^3P^0$	253.27	252.6	1.00	4.91[−02]	9.06[−02]	1.85	2[−04]
$3p^2$-$3s4f$ ^1D-$^1F^0$	263.16	260.7	0.99	1.82[−02]	8.68[−03]	0.48	0.356
$3s3d$-$3s5f$ ^3D-$^3F^0$	263.77	263.9	1.00	8.68[−02]	0.289	3.33	0.046
$3s3p$-$3s4s$ $^1P^0$-^1S	281.619	286.9	1.02	7.03[−03]	1.35[−03]	0.19	0.152
$3s4s$-$3s5p$ ^3S-$^3P^0$	290.21	290.5	1.00	1.48[−02]	3.37[−02]	2.28	1[−04]
$3s4p$-$3s6d$ $^3P^0$-^3D	299.68	301.1	1.00	0.314	0.613	1.95	0.025
$3s4p$-$3s7s$ $^3P^0$-^3S	302.6	303.5	1.00	0.162	0.104	0.64	0.028
$3s3d$-$3s8p$ ^1D-$^1P^0$	304.1	308.7	1.02	0.664	0.267	0.40	0.084
$3s3d$-$3s7f$ ^1D-$^1F^0$	307.4	312.8	1.02	1.18	1.20	1.02	0.019
$3s4p$-$3s6d$ $^1P^0$-^1D	308.852	312.8	1.01	1.65	0.394	0.24	0.036
$3s4p$-$3s7s$ $^1P^0$-^1S	313.5	317.8	1.01	0.251	4.36[−02]	0.17	0.01
$3s4s$-$3s5p$ ^1S-$^1P^0$	327.6	328.6	1.00	6.75[−02]	3.25[−02]	0.48	0.033
$3s3d$-$3s5p$ ^3D-$^3P^0$	331.5	330.4	1.00	2.70[−02]	4.59[−02]	1.7	0.009
$3s3d$-$3s7p$ ^1D-$^1P^0$	335.1	340.7	1.02	0.293	0.165	0.56	0.029
$3s3d$-$3s6f$ ^1D-$^1F^0$	342.8	349.5	1.02	0.699	0.608	0.87	0.003
$3s4p$-$3s5d$ $^3P^0$-^3D	365.3	367.7	1.01	0.209	0.381	1.82	0.091
$3s4p$-$3s5d$ $^1P^0$-^1D	370.322	375.1	1.01	0.864	0.160	0.19	0.13
$3s4p$-$3s6s$ $^3P^0$-^3S	373.59	374.6	1.00	0.121	6.32[−02]	0.52	0.027

TABLE III *(Continued).*

Transition	λ_{Lit} (nm)	λ_{OP} (nm)	$\frac{\lambda_{OP}}{\lambda_{Lit}}$	Δw_{SC} (nm)	Δw_{MSEM} (nm)	$\frac{\Delta w_{MSEM}}{\Delta w_{SC}}$	Oscillator strength
$3s4p$-$3s6s$ $^1P^0$-^1S	386.616	392.8	1.02	0.146	2.80[−02]	0.19	0.028
$3s3p$-$3p^2$ $^1P^0$-^1D	390.068	409.3	1.05	1.71[−02]	2.25[−03]	0.13	0.002
$3s3d$-$3s6p$ ^1D-$^1P^0$	402.6	410.5	1.02	0.218	9.59[−02]	0.44	0.009
$3s5s$-$3s8p$ ^3S-$^3P^0$	433.2	435.1	1.00	0.763	1.90	2.49	5[−05]
$3s5s$-$3s8p$ ^1S-$^1P^0$	462.9	462.3	1.00	1.54	0.879	0.57	0.014
$3p^2$-$3s4p$ ^1D-$^1P^0$	466.31	449	0.96	3.94[−02]	7.32[−03]	0.19	0.104
$3s4p$-$3s7p$ ^3D-$^3P^0$	537.1	540.2	1.01	0.548	1.25	2.28	0.002
$3s5d$-$3s7p$ ^1S-$^1P^0$	538.848	537.8	1.00	0.915	0.509	0.56	0.016
$3s4p$-$3s4d$ $^1P^0$-^1D	559.323	558.8	1.00	0.599	0.108	0.18	0.85
$3s5p$-$3s7d$ $^3P^0$-^3D	600.44	601.7	1.00	1.52	4.68	3.08	0.031
$3s5p$-$3s8s$ $^3P^0$-^3S	607.11	607.1	1.00	1.43	1.02	0.71	0.014
$3s4p$-$3s4d$ $^3P^0$-^3D	623.74	624.7	1.00	0.178	0.214	1.20	1.1
$3s3d$-$3p5p$ ^1D-$^1P^0$	633.574	653	1.03	0.232	0.118	0.51	0.05
$3s5s$-$3s6p$ ^3S-$^3P^0$	669.9	673.1	1.00	0.343	0.667	1.94	0.002
$3s4p$-$3s5s$ $^3P^0$-^3S	683.01	685.1	1.00	0.163	8.35[−02]	0.51	0.24
$3s4p$-$3s5s$ $^1P^0$-^1S	691.996	713.1	1.03	0.148	3.58[−02]	0.24	0.23
$3s4s$-$3s4p$ ^3S-$^3P^0$	704.93	699.8	0.99	7.82[−02]	5.01[−02]	0.64	1.31
$3s3d$-$3s4f$ ^1D-$^1F^0$	747.141	779.9	1.04	0.147	9.40[−02]	0.64	1.1
$3s5p$-$3s6d$ $^3P^0$-^3D	763.21	764.9	1.00	2.07	3.81	1.84	0.13
$3s4d$-$3s5f$ ^3D-$^3F^0$	835.82	849.9	1.00	1.12	2.81	2.51	0.74
$3s4s$-$3s4p$ ^1S-$^1P^0$	864.07	843.8	0.98	0.123	2.80[−02]	0.23	0.96

tion of interest. These are reduced to the dipole matrix element, multiplied by the Gaunt factor, and summed over. The function $g(x)$ is calculated using a linear interpolation of the known values for $2<x<50$ from Table I.

Once the linewidth is determined, the contribution of the line profile to the spectrum can be calculated assuming it to be a Lorentzian. As the MSEM is not sufficiently accurate to yield the line shifts, the lines are all centered about the unshifted wavelength of the transition. The ionization balance calculation, described above (Sec. III B) is used to give the populations of the upper states of the transitions. The line intensities are calculated using the degeneracies, A coefficients, and wavelengths given in the OP database.

IV. COMPARISON OF SEMICLASSICAL AND MSEM RESULTS

The significance of the use of the MSEM is twofold. First, it may be used to calculate spectra for which semiclassical calculations of the linewidths are not in the literature. This is particularly important for dense plasmas where spectral lines tend to be very broad and overlap. Second, with the ready

TABLE IV. Half widths at half maximum of some Al III lines, calculated at $N_e = 1 \times 10^{17}$ cm^{-3}, $T_e = 40\,000$ K, for both semiclassical and MSEM calculations. λ_{Lit} is the literature value for the transition [22], λ_{OP} the wavelength calculated by the Opacity Project [10], Δw_{SC} refers to the linewidth calculated from the semiclassical results [25], and Δw_{MSEM} refers to the widths calculated using the MSEM and OP database (this work). Configurations were taken from [24]. Powers of 10 are enclosed in brackets.

Transition	λ_{Lit} (nm)	λ_{OP} (nm)	$\frac{\lambda_{OP}}{\lambda_{Lit}}$	Δw_{SC} (nm)	Δw_{MSEM} (nm)	$\frac{\Delta w_{MSEM}}{\Delta w_{SC}}$	Oscillator strength
$3s$-$4p$	69.597	70.27	1.01	4.49[−04]	3.06[−04]	0.68	0.11
$3p$-$4d$	89.33	90.7	1.02	1.44[−03]	1.55[−03]	1.08	0.11
$3p$-$4s$	138.27	140.2	1.01	1.43[−03]	5.83[−04]	0.41	0.129
$3p$-$3d$	160.99	166	1.03	1.08[−03]	9.35[−04]	0.87	0.007
$3s$-$3p$	185.74	187	1.01	8.95[−05]	5.89[−04]	6.58	0.875
$3d$-$4f$	193.59	192.3	0.99	5.20[−03]	5.13[−03]	0.99	0.96
$3d$-$4p$	360.54	349.8	0.97	1.21[−02]	9.68[−03]	0.80	0.174
$4p$-$5s$	370.92	375.4	1.01	5.99[−02]	1.59[−02]	0.27	0.235
$4d$-$5f$	415.01	412.5	0.99	0.302	0.112	0.37	0.79
$4p$-$4d$	452.32	466.7	1.03	4.40[−02]	5.09[−02]	1.16	1.31
$4f$-$5d$	470.165	471.5	1.00	0.259	0.17	0.66	0.019
$4s$-$4p$	570.59	571.5	1.00	4.40[−02]	2.45[−02]	0.56	1.29

availability of the OP database, this method provides a rapid means of spectral synthesis for any element with $Z < 26$. Here we compare the semiclassical and MSEM spectra calculated in the visible region. These are compared with experimental data from a dense, warm aluminum plasma created by confined laser ablation.

A. Linewidths

Using the MSEM, we may calculate spectral linewidths. It is instructive to compare calculations from the current MSEM and semiclassical calculations. Previous studies [6,9] shared the average error in the linewidth to be ~50%. However, these studies used literature values for the atomic data. Thus a comparison of our calculations, using a consistent data set and semiclassical results, is useful. The results are summarized in Tables II–IV. Here the linewidths are calculated for $N_e = 10^{17}$ cm^{-3}. This is to allow a direct comparison between the MSEM results and extant widths calculated using the semiclassical method, avoiding errors associated with extrapolation of the semiclassical widths to higher density, where Debye shielding, for example, may be important. We find that for the ionized species, the MSEM and semiclassical calculations are within ~100%. This is greater than is generally accepted for the MSEM. The reason for this increase in the error is not clear. It is likely that it is due to differences in the atomic data used [9]. For the neutral, the situation is much worse, the average error being around 200%. This is because the threshold and effective Gaunt factors used are not suitable for the neutral. The threshold value for neutral excitation is 0 [19], and it rises more rapidly than for ions. Previous studies of the MSEM using the neutral threshold have shown an underestimation of a factor of 1.5 in the width [20].

We may examine certain of the results from ions in more detail. For example, results for the 570-nm Al III line ($4p$-$4s$) are shown in Table V. For this line, $E/\Delta E = 0.6$, and the unmodified semiempirical model, based on Eqs. (8) and (7) above, should be valid. As g does not increase above its threshold value for this transition, $\tilde{g}$ is also at its threshold value of 0.53 for a doubly ionized line. Thus the matrix elements for $\Delta n = 0$ transitions are not greatly enhanced by the move to the MSEM, and so the small difference in the linewidths calculated with the OP data is unsurprising. It is harder to reconcile this with the larger increase of the other calculation [9], which is presumed to be due to a difference in the atomic data used.

B. Comparison of calculated spectra

We can compare the full spectra calculated from the semiclassical data and the MSEM directly. Spectra calculated for an aluminum plasma at 2×10^{19} cm^{-3} and 25 000 K using the two methods are shown in Fig. 1. It can be seen that, in general, some agreement between the two is found. The lack of shifts and inaccuracies in the central wavelength of the MSEM method and the OP database are observable. Additionally, the MSEM-OP method has a much higher continuum, which is particularly apparent in the infrared region of the spectrum. This is due to the very broad lines which the code calculates, which underlie the entire spectrum. In order to compare the calculated spectra more exactly, we may use a reduced OP database, consisting of only those transitions for which semiclassical broadening data are available. The spectrum calculated at 2×10^{19} cm^{-3} and 25 000 K using this reduced OP database and the MSEM method is com-

TABLE V. Comparison of results for the Al III 570-nm line. SEM refers to calculations using Eqs. (8) and (7) above. The MSEM-Bates–Damgaard method refers to Eqs. (9)–(11) above.

Calculation	Δw (nm)	Reference
MSEM-OP	2.44×10^{-2}	This work
Semiclassical	4.4×10^{-2}	[25]
MSEM-Bates–Damgaard	3.76×10^{-2}	[9]
SEM	2.31×10^{-2}	[9]
SEM	2.17×10^{-2}	This work

pared with the semiclassical spectrum in Fig. 2. It can be seen that the agreement between the calculations is improved.

The feature in Figs. 1 and 2 labeled Al II 365-nm $3s4p$-$3s5d$ is in fact a blend of three Al II lines. These are 365 nm ($3s4p$-$3s5d$), 374 nm ($3s4p$-$3s6s$), and 370 nm ($3s4p$-$3s5d$). The 365-nm line is dominant, but roughly half the total intensity comes from the other two lines. The difference in continuum level between the spectrum calculated with the full OP data set shown in Fig. 1 and the semiclassical and reduced OP data set spectra is most apparent on the blue edge of the spectrum. This is due to a very broad Al II feature, which is a combination of lines, mainly Al II, 219 nm ($3p3d$-$3s3d$) which is not included in the semiclassical calculations. This shows that the calculation of the entire spectrum is necessary when the spectral features can be this broad. Further work would be required to establish if the calculated width of the Al II 219-nm line is correct.

C. Comparison of experimental and calculated spectra

Recent experiments obtained spectra in the visible region from a dense ($N_e \sim 2\times10^{19}$ cm^{-3}), warm ($T \sim 2-5$ eV) Al spectrum [1]. In the observed spectra, lines from Al I, II, and III have been identified. The lines, at the high densities of the plasma, are very broad, and merge into each other. A calculation, using the Saha-Boltzmann equation for the ionization balance and semiclassical linewidths from the literature, was written to interpret the spectrum [12]. It is of great interest to compare these results with those of the MSEM using the OP database. In all cases there are two criteria to be met in deciding the best fit. First, we use the least-squares fit of the calculated spectrum, suitably scaled, to the data. Second, we require those lines which are observed in the data to be also present in the calculation. This places a restriction on the permitted values of Z^*. Within this, the errors are found from the range over which reasonable fits are obtained, usually within a range of 5% of the least-squares parameter.

The experimental data are shown in Fig. 3. These were obtained 70 ns after the laser shot in a confined plasma ablation [1]. The plasma, at this time, should be at its hottest and most dense, and the homogeneity should be high. Originally, the plasma was diagnosed for density using the linewidths from the semiclassical method. Although it proved to be difficult to measure the linewidths from the data with high accuracy, a density of $(2.4\pm0.8)\times10^{19}$ cm^{-3} was inferred. The temperature was obtained by finding the closest fit of the calculated semiclassical spectrum to the data. This yields a temperature of $40\,000\pm5000$ K. Figure 3 also shows the closest fit of the semiclassical code. It should be noted that there is a systematic error of ~5 nm in the wavelength calibration of the data, which has been corrected by offsetting the calculated spectrum.

The original density diagnostic was obtained by measuring the width of three lines. The density obtained from these lines and from the widths derived from the MSEM are shown in Table VI. Clearly, we cannot rely on the MSEM linewidths to provide an accurate density diagnostic, as the scatter in the densities derived from the linewidths is great. The accuracy of an individual linewidth, calculated from the MSEM, upon which the density diagnostic relies, is poor. It should also be noted, however, that the difficulties presented by the data are large in this case as the 452-nm line ($4p$-$4d$) has an obscured blue wing, and has the Al II 466-nm line ($3p2$-$3s4p\ ^1D$-$^1P^0$) underlying the red wing. As noted below, neither the semiclassical nor MSEM calculation reproduces the spectrum around the 570- and 623-nm lines. In some cases, for the semiclassical calculation, we

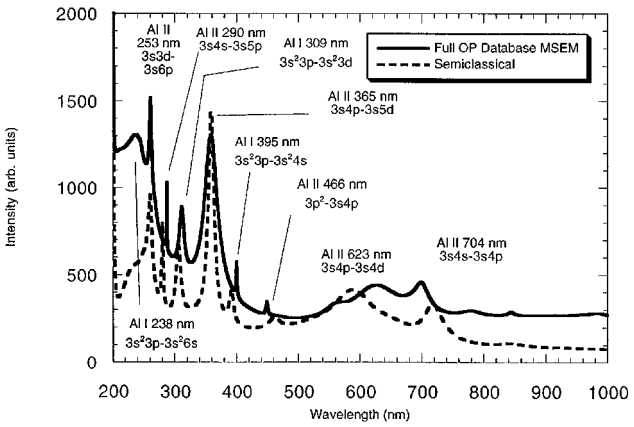

FIG. 1. Comparison of the results of the MSEM code and the semiclassical code for aluminium at 2×10^{19} cm^{-3}, 25 000 K.

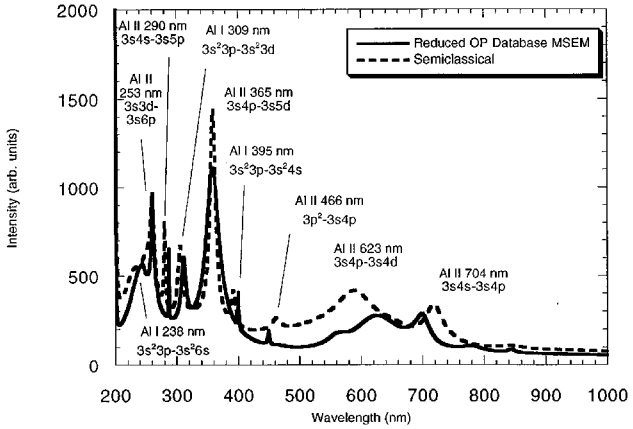

FIG. 2. Comparison of the results of the reduced data set MSEM code and the semiclassical code for aluminium at 2×10^{19} cm^{-3}, 25 000 K.

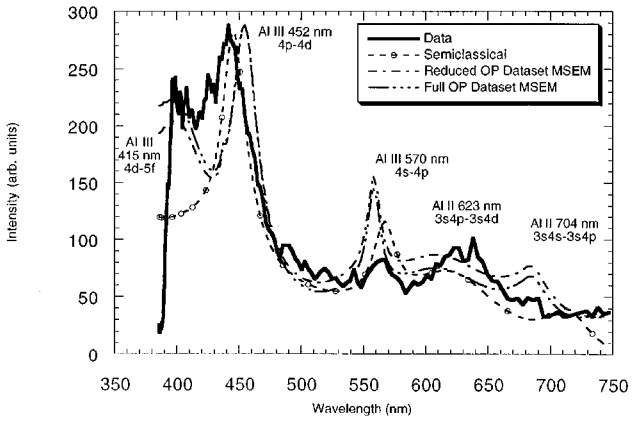

FIG. 3. Comparison of the results of experimental data, the full data set MSEM code, the reduced data set MSEM code, and the semiclassical code for aluminium at 2.5×10^{19} cm^{-3}, 40 000 K.

TABLE VI. Density diagnostics from linewidths for the semiclassical and MSEM data.

Ion stage	Transition	Wavelength (nm)	Experimental HWHM (nm)	Semiclassical N_e (10^{19} cm^{-3})	MSEM N_e (10^{19} cm^{-3})
Al III	$4s$-$4p$	570	11.7	2.66	4.77
Al III	$4p$-$4d$	452	14.4	3.27	2.82
Al II	$3s4p$-$3s4d$ $^3P^0$-^3D	623	23.3	1.37	0.99
Average				2.4 ± 0.8	2.9 ± 1.5

may also have confirmation of the density diagnostic from measurement of the shift of a spectral line, particularly the neutral where the shifts are large [11].

We find that the errors in the densities can be reduced somewhat by using the overall spectral fit of the experimental and calculated data, which negates the overlap problems and leads to a slight reduction of the error in the semiclassical fit. This is due to the variation of Z^* with electron density. The best semiclassical fit for the electron density to the spectrum in Fig. 3 is $N_e=(2.5\pm0.5)\times10^{19}$ cm^{-3}. We may also undertake this procedure for the MSEM-OP calculation. The method by which this reduction is obtained is exemplified in Fig. 4, where the spectra generated by the mean and extremes of the standard deviation of the linewidth density diagnostic are shown. Clearly, taking the upper limit, the 623-nm Al II line ($3s4p$-$3s4d$) is not reproduced at all, and so this limit is too high, particularly as the feature around 450 nm is too broad. Thus a reduction of the upper limit of the electron density is required. Similarly for the lower limit all lines are too narrow, and the dip at around 400 nm in the spectrum is too low. Hence an increase of the lower limit of the electron density is needed to reproduce the spectrum. In this case a result of $N_e=(2.5\pm0.5)\times10^{19}$ cm^{-3} is found. This result is shown in Fig. 5 using the reduced OP data set at a temperature of 40 000 K. A much closer fit to the data is found from this diagnostic than from the linewidths alone. This is the basis of the use of Z^* in the diagnosis referred to above.

We can fit the spectrum at the diagnosed density and obtain the plasma temperature. The semiclassical fit yields $40\,000\pm5000$ K. This is shown in Fig. 6, using the reduced data set MSEM code for the fits. The electron density chosen is 2.5×10^{19} cm^{-3}. Shown in Fig. 3 are the calculated spectra from the MSEM code for both the reduced and full OP data set at 2.5×10^{19} cm^{-3}. These also yield temperatures of $40\,000\pm5000$ K.

It is of interest to note that the agreement between both MSEM generated spectra and the data is better than between the semiclassical data. This is because the Al III 415.01-nm line ($4d$-$5f$) is calculated to be narrower by the MSEM than by the semiclassical (Table IV). The overall intensity of the line is the same in both cases, indicating that the difference is entirely due to the different linewidths. Thus the utility of the MSEM code is established. It should also be noted that the semiclassical code is closer than the MSEM in the linewidth of the Al III 570-nm line ($4s$-$4p$), and that neither of the codes does particularly well in this region. Shifts are not included in the MSEM code, as the cancellations of the shift from states above and below the state of interest make the MSEM even less reliable. It will be observed that the position of the peak at $\sim$450 nm in the MSEM spectrum is not correct. The main transition here is the Al III line at 452 nm ($4p$-$4d$). The apparent shift is due to the inaccuracy of the central wavelength position of this transition in the OP-database (Table IV) where the position of the line is $\sim$14 nm from the observed location.

V. CONCLUSIONS

We find that the MSEM with the OP database is a fast and reasonably reliable method for producing spectra. A comparison between semiclassical and MSEM linewidths for ion

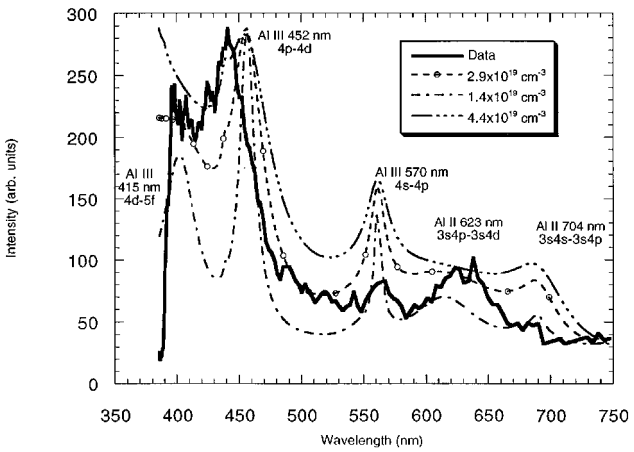

FIG. 4. The MSEM spectrum for the extremes of the linewidth diagnostic using MSEM linewidths (Table VI) at 40 000 K.

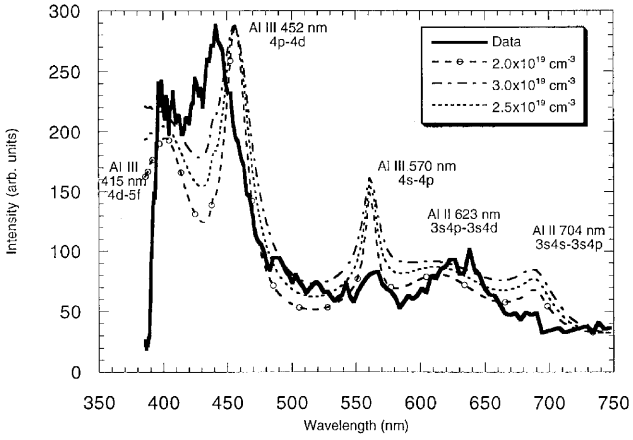

FIG. 5. The best-fit MSEM spectrum, at 40 000 K, showing the improvement in agreement with experimental data obtained using a fit of the entire spectrum.

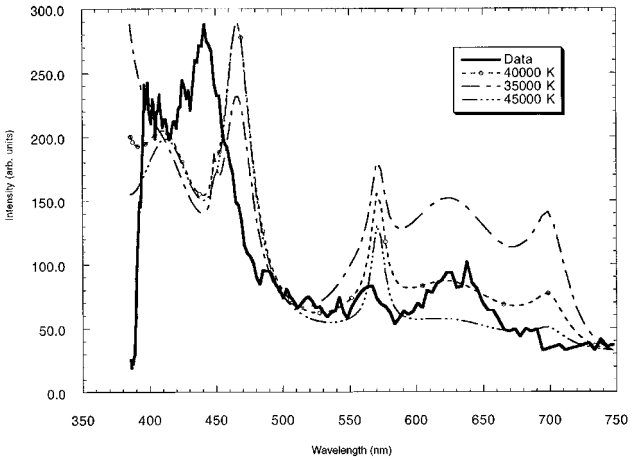

FIG. 6. The MSEM temperature fits, using the reduced data set MSEM code. Fits are shown at $T=35\,000$, 40 000, and 45 000 K.

lines indicates that there is a mean difference of $\sim 100\%$ in linewidth compared to semiclassical calculations. For the neutral lines, the error is greater, and no reliance should be placed on the MSEM calculated lines, as the method implemented here is not appropriate. We find that a density diagnostics based on the linewidth alone is subject to considerable error, but that fitting an entire region of the spectrum yields a more reliable result.

The advantages of the MSEM coupled to the OP database are those of speed and range of data available. While the semiclassical code is actually faster to run in pure computation time, the time required to assemble the required atomic and linewidth data is much greater. The range of data available from the OP data base is also much more comprehensive than that which is generally found in already extant data compilations. Thus, while the full MSEM code may take longer to run, the assembly of data is orders of magnitude faster. If there were a suitable database and program for the semiclassical method, capable of calculating the ionization balance and line shapes, in a reasonable manner, then the method presented here would not be useful. However, although fast line-shape codes exist, such as TOTAL [21], they cannot also at present calculate the ionization balance and relative intensities of all the ionization stages required. Additionally, a typical Al I line takes 1-min CPU time on a DEC Alpha machine using TOTAL with Opacity Project input atomic data, whereas the computing time on a desktop Power PC-type machine for the same line is about 0.24 s using the MSEM with the same input data. While the latter method does not have the accuracy or the detailed line shape of the former, the sheer quantity of data to be processed indicates that the MSEM method is the most viable.

The spectral fits of the MSEM data using the OP database are in reasonable agreement with those generated using the literature values of the linewidths from the semiclassical method. While the individual linewidths are poor for the MSEM, the overall spectrum is as accurate, and in some cases provides a better fit to the data. The coupling of the MSEM with the Opacity Project atomic database gives a set of reliable atomic structure and transition data, which yields good quality spectra. Improvements in the wavelength accuracy of the transition data would be useful, as while the average accuracy is high, a few lines are much further away from their observed position. This is likely to have an effect on the line broadening calculations, as it implies that the energy differences between the states are not exact.

In summary, we tested a fast spectral simulation model based on the modified semiempirical method for the linewidths, the Saha-Boltzmann equation for the ionization balance, and atomic data provided by the Opacity Project database. We find that, under the circumstances tested, this method provides a good diagnostic of a dense plasma. The diagnostics from the MSEM were comparable in accuracy to those obtained using literature values of the linewidths and atomic data from various sources in a similar calculation. This gives confidence that, for an element where there are few semiclassical calculations of linewidths extant, the modified semiempirical method, coupled to a reliable atomic database, is a reasonable first step in developing a diagnostic capability. A detailed description of the code and its data requirements is currently being prepared. The code will be made generally available with this latter publication.

ACKNOWLEDGMENT

This work was performed under EPSRC Grant No. GRK 96236.

[1] D. J. Heading, G. R. Bennett, J. S. Wark, and R. W. Lee, Phys. Rev. Lett. **74**, 3616 (1995).
[2] A. N. Mostovych, K. J. Kearney, J. A. Stamper, and A. J. Schmitt, Phys. Rev. Lett. **66**, 612 (1991).
[3] D. Riley, L. A. Gizzi, F. Y. Khattak, A. J. Mackinnon, S. M. Viana, and O. Willi, Phys. Rev. Lett. **69**, 3739 (1992).
[4] A. C. Kolb and H. R. Griem, Phys. Rev. **111**, 514 (1958).
[5] M. Baranger, Phys. Rev. **111**, 494 (1958).
[6] H. R. Griem, Phys. Rev. **165**, 258 (1968).
[7] H. R. Griem, *Spectral Line Broadening By Plasmas* (Academic, New York, 1974).
[8] M. S. Dimitrijevic and N. Konjevic, in *Spectral Line Shapes 9*, edited by B. Wende (de Gruyter Berlin, 1981), pp. 211–239.
[9] M. S. Dimitrijevic, Bull. Obs. Astron. Belgrade **139**, 31 (1988).
[10] M. J. Seaton, *The Opacity Project* (Institute of Physics Publishing, Bristol, 1995), Vol. 1.
[11] M. S. Dimitrijevic and N. Konjevic, J. Quant. Spectrosc. Radiat. Transf. **24**, 451 (1980).
[12] D. J. Heading, G. R. Bennett, J. S. Wark, and R. W. Lee, J. Quant. Spectrosc. Radiat. Transf. **54**, 167 (1995).
[13] H. A. Bethe, Ann. Phys. (Leipzig) **5**, 3251 (1930).
[14] H. R. Griem, M. Baranger, A. C. Kolb, and G. Oertel, Phys. Rev. **125**, 177 (1962).
[15] D. R. Bates and A. Damgaard, Philos. Trans. R. Soc. London, Ser. A **242**, 101 (1949).

[16] G. K. Oertel and L. P. Shomo, Astrophys. J. Suppl. Ser. **16**, 175 (1968).
[17] J. C. Stewart and K. D. Pyatt, Astrophys. J. **144**, 1203 (1966).
[18] *Atomic Energy Levels & Grotrian Diagrams I. Hydrogen I-Phosphorous XV*, edited by S. Bashkin and J. O. Stoner, Jr. (North-Holland, New York, 1975), pp. 440–457.
[19] M. J. Seaton, in *Excitation and Ionisation by Electron Impact. Atomic and Molecular Processes*, edited by D. R. Bates (Academic, New York, 1962), pp. 375–420.
[20] M. H. Miller and R. D. Bengtson, Phys. Rev. A **1**, 983 (1970).
[21] A. Calisti, L. Godbert, R. Stamm, and B. Talin, J. Quant. Spectrosc. Radiat. Transf. **51**, 59 (1994).
[22] W. L. Wiese, M. W. Smith, and B. M. Miles, *Atomic Transition Probabilities: Sodium Through Calcium* (National Bureau of Standards, Washington D.C., 1969), Vol. 2.
[23] H. R. Griem, *Plasma Spectroscopy* (McGraw-Hill, New York, 1964).
[24] V. Kaufman and W. C. Martin, J. Phys. Chem. Ref. Data **20**, 775 (1991).
[25] M. S. Dimitrijevic, Z. Djuric, and A. A. Mihajlov, J. Phys. D **27**, 247 (1994).